Bioconjugate Chemistry

Article

Cite This: Bioconjugate Chem. 2017, 28, 2729-2736

pubs.acs.org/bc

Tuning the Multifunctionality of Iron Oxide Nanoparticles Using Self-Assembled Mixed Lipid Layers

Matthew R. Preiss,[†] Eily Cournoyer,[†] Karissa L. Paquin,[‡] Elizabeth A. Vuono,[‡] Kayla Belanger,[†] Edward Walsh,[§] Niall G. Howlett,[‡] and Geoffrey D. Bothun*[,†]

[†]Department of Chemical Engineering, University of Rhode Island, 51 Lower College Road, Kingston, Rhode Island 02881, United States

[‡]Department of Cell and Molecular Biology, University of Rhode Island, 379 CBLS, 120 Flagg Road, Kingston, Rhode Island 02881, United States

[§]Department of Neuroscience, Department of Diagnostic Imaging, Institute for Brain Science, Institute for Molecular and Nanoscale Innovation, Associate Director for MRI Physics, Brown University, Sidney E. Frank Hall, 185 Meeting Street, Providence, Rhode Island 02912, United States

ABSTRACT: We present an approach to tuning the multifunctionality of iron oxide nanoparticles (IONs) using mixed self-assembled monolayers of cationic lipid and anionic polyethylene glycol (PEG) lipid. By forming stable, monodispersed lipid-coated IONs (L-IONs) through a solvent-exchange technique, we were able to demonstrate the relationship between surface charge, the magnetic transverse relaxivity (r_2 from T_2-weighted images), and the binding capacity of small interfering ribonucleic acids (siRNAs) as a function of the cationic-to-anionic (PEG) lipid ratio. These properties were controlled by the cationic charge and the PEG conformation; relaxivity and siRNA binding could be varied in the mushroom and brush regimes but not at high brush densities. In vitro results combining cell viability, uptake, and transfection efficiency using HeLa cells suggest that the functional physicochemical and biological properties of L-IONs may be best achieved using catanionic lipid coatings near equimolar ratios of cationic to anionic PEG−lipids.

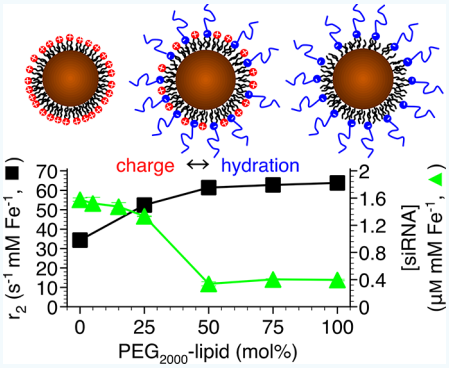

INTRODUCTION

Iron oxide nanoparticles (IONs) can achieve multiple therapeutic objectives including imaging, drug delivery, gene therapy, and localized hyperthermia.[1−5] Designing a common ION capable of achieving multiple objectives requires design parameters that relate the physicochemical properties of a ION to their functionality. ION surface modification and ligand composition are particularly important because they govern, among many properties, the surface charge and the nature of the hydration shell.[6,7] These parameters, in turn, influence the colloidal stability, the magnetic relaxivity or magnetic resonance imaging (MRI) contrast,[8−13] and the adsorption behavior of therapeutic molecules such small interfering ribonucleic acid (siRNA)[14,15] of the IONs.

Nanoparticle ligands often include polyethylene glycol (PEG), which is a hydrophilic biocompatible polymer used to improve the blood circulation half-life and reduce nanoparticle cytotoxicity.[16−19] For IONs, PEG ligands also influence the magnetic relaxivity, and mixed results have been reported. IONs exhibit high transverse relaxivity (r_2), or negative MRI contrast (in T_2 weighted images) that are due to the induced ION magnetic dipolar field slowing the dipole relaxation rate of protons (water) nears the ION surface. Tong et al.[11] have shown that PEG−lipids assembled on 14 nm superparamagnetic IONs with low PEG molecular weights (up to 1000 MW) yield high r_2 values, while high PEG molecular weights (2000 and 5000 MW) yield low r_2 values. Increases in r_2 have also been observed as the PEG molecular weight was increased from 300 to 750 MW over a range of ION diameters.[9−11] A pair of competing factors have been proposed: reduced water diffusivity in PEG coatings with low molecular weights, leading to high r_2 values, and water exclusion from PEG coatings with high molecular weights leading to low r_2 values. The transition between high and low r_2 values with PEG molecular weight remains an open question and is dependent upon ION size and saturation magnetization.

ION relaxivity studies with PEG coating thickness have been limited to single PEG ligand layers. However, mixed ligand layers containing PEG ligands are commonly used to create functional nanoparticles for biomedical applications.[20−22] The additional ligand component(s) can be used for adsorbing molecules such as siRNA. IONs, in particular, have attracted interest for directed siRNA delivery using a cationic lipid to drive siRNA binding.[14,15] IONs containing mixed PEG and cationic ligand layers represent a unique system with which to study the design parameters required to maximize multiple

Received: August 11, 2017
Revised: October 4, 2017
Published: October 16, 2017

DOI: 10.1021/acs.bioconjchem.7b00483
Bioconjugate Chem. 2017, 28, 2729−2736

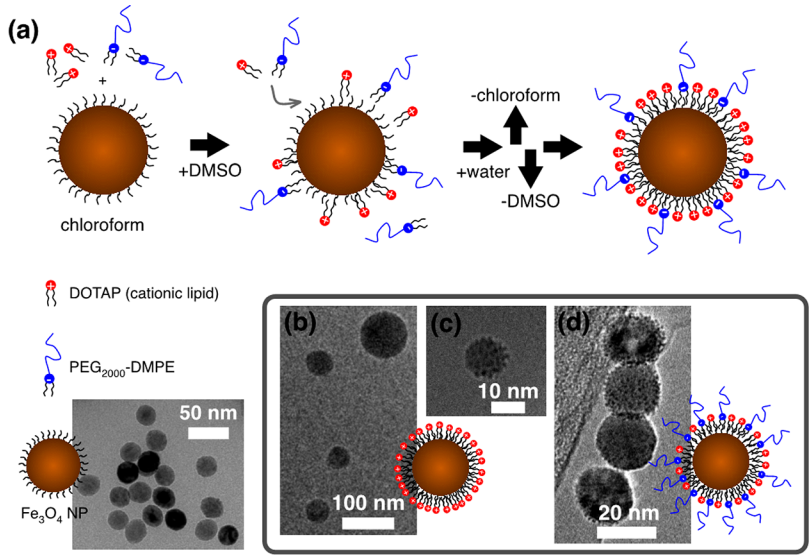

Figure 1. L-ION formation and cryo-TEM analysis. (a) Dual solvent exchange process in which DMSO is used as a solvent bridge between chloroform and water to control the self-assembly of the mixed ligand layer (DOTAP and PEG_{2000}–DMPE). Chloroform was removed by rotary evaporation, and DMSO was removed by centrifugal ultrafiltration. The TEM micrograph shows native IONs dried from chloroform. Representative cryo-TEM micrographs of L-IONs at (b) 0 mol %, (c) 15 mol %, and (d) 50 mol % PEG_{2000}–DMPE. PEG groups are visible as globule-like structures on the L-ION surfaces at 15 and 50 mol % PEG_{2000}–DMPE.

therapeutic objectives (in this case, MRI imaging and siRNA delivery). Huang et al.[13] have shown that 10 nm superparamagnetic IONs coated with 1,2-dioleoyl-3-trimethylammonium-propane (chloride salt) (DOTAP) and 1,2-distearoyl-*sn*-glycero-3-phosphoethanolamine–*N*-[methoxy(polyethylene glycol)-2000] (ammonium salt) (PEG_{2000}–DSPE) at a ratio of 3:1 achieve high cellular uptake and can be used for MRI in vivo. In this work, the mixed ligand composition was constant, and the relaxivity mechanisms were not examined. Ligand composition, specifically the ratio of cationic to PEG ligands, is an important variable because it will control PEG conformation and surface charge density. These parameters provide a new approach to tuning magnetic relaxivity and siRNA binding.

We have employed a dual solvent exchange (DSE) method to prepare monodispersed lipid-coated iron nanoparticles (L-IONs) containing mixed layers of self-assembled cationic DOTAP and 1,2-dimyristoyl-*sn*-glycero-3-phosphoethanolamine–*N*-[methoxy(polyethylene glycol)-2000] (ammonium salt) (PEG_{2000}–DMPE or PEG–lipid) as a function of the lipid ratio. The phosphate group of DMPE possesses a negative charge rendering an anionic PEG–lipid. As a result, coatings with DOTAP/PEG–lipid mixtures are catanionic near the ION surface, between lipid groups, with nonionic PEG groups extending from the surface.

In addition to examining the physicochemical, siRNA binding, and relaxivity properties of the L-IONs as a function of the cationic-to-PEG–lipid ratio, we also examine cellular uptake and siRNA transfection in vitro using L-IONs at concentrations that did not reduce cell viability. Transfection was performed with nontargeting fluorescent siRNA and siRNA targeting FANCD2,[23] which is one of the proteins involved in the Fanconi anemia and BRCA responsible for the repair of deoxyribonucleic acid (DNA) interstrand cross-links. DNA repair is one mechanism of resistance to DNA cross-linking chemotherapeutics.

RESULTS AND DISCUSSION

In the modified dual solvent exchange method, dimethyl sulfoxide (DMSO; dielectric constant, ε = 46.7) acts as a miscible solvent bridge between chloroform (ε = 4.8) and water (ε = 80.1).[24] Through DSE, hydrophobic oleic acid-coated IONs (Figure 1a) were coated with self-assembled mixed monolayers of cationic DOTAP and anionic PEG_{2000}–DMPE at different DOTAP-to-PEG_{2000}–DMPE ratios. Cryo-transmission electron microscopy (TEM) images of L-IONs at three conditions (0, 15, and 50 mol % PEG–lipid) are shown in panels b–d of Figure 1, respectively. Globule-like structures can be seen extending from the L-MNP surface when PEG–lipid was present. The structures observed are consistent with previous cryo-TEM observations for PEG brushes on block copolymer micelles.[25]

Effect of PEGylation on Physicochemical and Magnetic Properties. The dual solvent exchange method has been shown to yield monodisperesed L-IONs coated with PEG–lipid.[24] We show that this method is also yields monodispersed particles with cationic and anionic PEG and lipid mixtures. Native IONs in chloroform had a number-averaged hydrodynamic diameter, D_H, of 28.3 nm. For L-IONs in water, the D_H ranged from 30.9 to 34.6 nm across all PEG–lipid concentrations (Figure 2a), equivalent to a lipid coating thickness between 1.3 and 3.2 nm.

By varying the PEG–lipid concentration, a broad range of L-ION surface charge could be obtained as depicted by the ζ potential, which began at +64.8 mV (all DOTAP) and decreased to −35.1 mV (all PEG–lipid; Figure 2a). A total of three different regions were observed in the ζ: (i) a modest decrease in ζ up to 25 mol % PEG–lipid, (ii) a significant decrease in ζ and charge reversal between 25 and 50 mol % PEG–lipid, and (iii) large negative ζ at and above 75 mol % PEG–lipid. As the PEG–lipid concentration increases and the anionic phosphate group in the PEG–lipid dominates the surface charge.

DOI: 10.1021/acs.bioconjchem.7b00483
Bioconjugate Chem. 2017, 28, 2729–2736

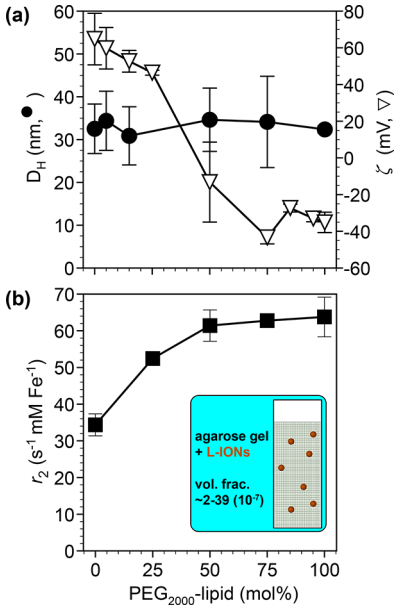

Figure 2. L-ION properties as a function of the PEG−lipid concentration. (a) Hydrodynamic diameter, D_H, and ζ potential; (b) transverse relaxivity, r_2, measured by MRI at 3 T and 20 °C. Error bars represent standard deviation for $n \geq 3$, and the error bars not visible are smaller than the symbol size.

In addition to changing the L-ION surface charge, the presence of PEG−lipid altered the hydration shell and, in turn, the magnetic proton relaxivity of water surrounding the IONs. MRI measurements of relaxivity scanned at 3 T and 20 °C were used to further reveal the structure of mixed ligand layers. The transverse relaxivity (r_2; negative MRI contrast) was examined in agarose gels containing dispersed L-IONs and determined as:

$$r_2 = (1/T_2 - 1/T_{2,\text{water}})/C_{\text{Fe}} \quad (1)$$

where T_2 is the transverse relaxation rate and C_{Fe} is the iron concentration. The r_2 values increased with PEG−lipid concentration up to 50 mol % and then plateaued (Figure 2b). The increase in r_2 suggests that the PEG coating did not yield an impermeable shell as previously proposed for PEG-coated superparamagnetic IONs.[10,11] Rather, a denser hydration shell was present within the PEG layer, where the magnetic field inhomogeneity caused by the L-IONs increased the dephasing of bound water protons.

Compared with commercial iron oxide based contrast agents (Feridex, r_2 = 98.3 s^{-1} mM^{-1}; Resovist, r_2 = 151 s^{-1} mM^{-1}; and Ferumoxtran-10, r_2 = 151 s^{-1} mM^{-1}),[26] L-IONs exhibited lower to comparable transverse relaxivity at PEG−lipid concentrations of ≥50%. Where L-IONs did outperform commercial agents was in the ratio of r_2 (negative contrast) to the longitudinal relaxivity (r_1, positive contrast). Longitudinal relaxivity was only observed at 75 mol % and 100 mol % PEG−lipid, and the ratio of r_2 to r_1 was 50 and 29, respectively. r_1 could not be measured below 75 mol % PEG−lipid. Reported r_2-to-r_1 ratios for Feridex, Resovist, and Ferumoxtran-10 exhibit are approximately 4, 5, and 6, respectively. L-IONs exhibit greater negative contrast efficiency than these commercial agents based on the higher r_2-to-r_1 ratios.[27]

When relaxivity falls within the motional average regime (MAR), also referred to as the outer-sphere theory, r_2 values are a function of ION size and the water diffusivity near the ION surface, expressed as the translational diffusion time of a proton across a ION ($\tau_D = d^2/4D$ where d is the L-ION diameter and D is the water diffusivity). A hydrated surface coating can give rise to an effectivity water diffusivity that can lead to increases in r_2, i.e., proton diffusivity is slower near an ION and the proton experiences increased dephasing by the ION magnetic dipole.[28] r_2 can be determined as:[29,30]

$$r_2 = \frac{16}{45} \nu_{\text{mat}} \tau_D (\Delta\omega)^2 \quad (2)$$

where ν_{mat} is the iron molar volume derived from the volume fraction of IONs within the sample and $\Delta\omega$ is the angular frequency shift of a proton at the ION equator. For the L-IONs, ν_{mat} and $\Delta\omega$ were dependent on the ION properties and constant. r_2 can therefore be expressed as $r_2 = C\tau_D = C(d^2/4D)$ where $C = (16/45)\nu_{\text{mat}}\Delta\omega$. From this expression, the effective water diffusivity in the PEG layers (D_{eff}) can be estimated by assuming that the L-ION size is constant and that the water diffusivity near a L-ION coated with DOTAP (no PEG−lipid) is unaffected by the DOTAP coating (Table 1). These assumptions yield the relationship $(r_{2,\text{DOTAP}}/r_2) = (D_{\text{eff}}/D)$ where $r_{2,\text{DOTAP}} \propto 1/D$ and $r_2 \propto 1/D_{\text{eff}}$.

Table 1. Transverse Relaxivity and Calculated Effective Diffusivity

PEG−lipid (mol %)	r_2 (s^{-1} mM Fe^{1-})	D_{eff} (10^{-9} m^2 s^{-1})
0	34.3 ± 2.1	2[a]
25	52.4 ± 0.8	1.31
50	61.4 ± 3.0	1.12
75	62.8 ± 0.3	1.09
100	63.8 ± 3.8	1.08

[a]Water diffusivity (D) at 20 °C, assumed to be unaffected by a DOTAP coating.

Based on D_{eff}, water diffusion was hindered near the L-ION surface as the PEG density increased up to 50 mol % PEG−lipid, leading to higher r_2 values (Figure 3). This finding

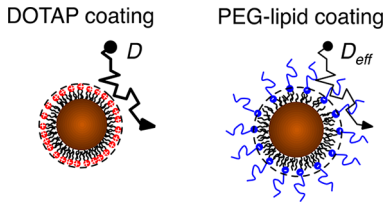

Figure 3. Water diffusion near the L-ION surface when coated with DOTAP or PEG−lipid. The PEG−lipid coating leads to an effective (hindered) water diffusivity, D_{eff}, compared to the DOTAP coating.

suggests that the PEG coating is not impermeable to water and that it does not reduce the distance of closet approach between a proton and the ION surface (compared to L-IONs with a DOTAP coating) as reported for other PEG-coated magnetic nanoparticles.[11,31]

The physicochemical and relaxation properties of the L-IONs are dependent upon the structure of the mixed ligand layer (specifically, the PEG−lipid density and conformation). To estimate PEG−lipid conformation, the distance between PEG−lipids on the L-ION surfaces (D) was initially calculated based on the lipid ratio and the area-per-headgroup (A) for DOTAP (0.65 nm^2) and DMPE (0.52 nm^2) (Figure 4).[17,32] This assumes that PEG does not alter the packing of DMPE

DOI: 10.1021/acs.bioconjchem.7b00483
Bioconjugate Chem. 2017, 28, 2729−2736

within the monolayer, which is not correct at high PEG–lipid concentrations, as discussed below.

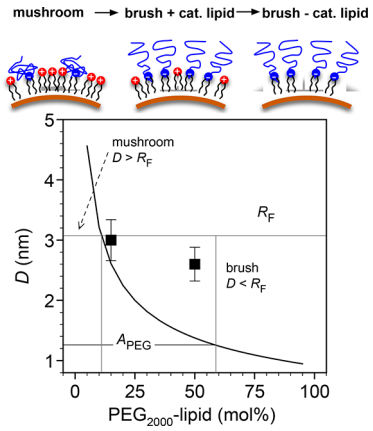

Figure 4. Theoretical PEG surface spacing, D, as a function of PEG–lipid concentration. D is compared to the Flory radius, R_F, and the PEG_{2000}–DMPE area-per-lipid, A_{PEG}. Theoretical mushroom and brush regimes are shown; the gray region denotes where the lipid tails intercalate with the oleic acid (not shown) on the ION surface. The data points are based on cryo-TEM measurements of D. The standard deviation is for $n \geq 10$.

Comparing D to the Flory radius (R_F) indicates that the mushroom to brush transition occurred at ~10 mol %. Measurements of D based on cryo-TEM at 15 mol % PEG–lipid are in close agreement with the calculations and suggest that the globule-like structures were PEG brushes. At 50 mol % PEG–lipid a lower D was measured, consistent with a denser PEG brush, but D was greater than the calculated value. Based on the reported area-per-headgroup for PEG_{2000}–DMPE in which PEG is in a brush conformation (A_{PEG} = 1.26 nm^2), the maximum PEG–lipid packing that could be achieved would occur when $A_{PEG} = D$. This condition corresponds to ~57 mol % PEG–lipid, above which additional PEG–lipid would not "fit" within the coating due to steric hindrances. This is in agreement with the plateaus observed for ζ potential and r_2 above 50 mol % PEG–lipid.

Effect of PEGylation on siRNA Binding. L-ION PEGylation leads to charge reversal and increased r_2. These properties are governed by PEG–lipid density and PEG conformation, which should be reflected in siRNA binding.

With the use of a quenching assay with FAM-labeled siRNA (Figure 5a), in which siRNA binding to cationic lipids causes fluorescence quenching,[33,34] the siRNA binding capacity closely mirrored the ζ potential results and was driven by electrostatic attraction at high DOTAP concentrations when PEG was in mushroom (5 mol % PEG–lipid) and brush conformations (15 and 25 mol % PEG–lipid) (Figure 5b). In these mixed ligand layers, electrostatic attraction dominated and PEG did not prevent siRNA binding. Low siRNA binding was observed at high PEG–lipid concentrations, and results from 50 to 100 mol % were statistically the same, suggesting that the brushes were saturated at these conditions (i.e., a dense brush in which brush densities were similar near and above $A_{PEG} = D$). Reduced siRNA binding with increased PEG concentration was expected as PEG is known to reduce nonspecific surface adsorption.

Effect of PEGylation on Cell Viability, Uptake, and Transfection in Vitro. L-IONs with mixed ligand layers containing 0 to 50 mol % PEG–lipid exhibit high r_2 and high

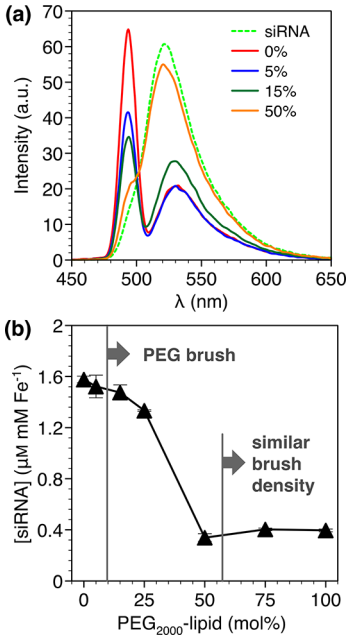

Figure 5. FITC–siRNA binding to L-IONs. (a) Fluorescence spectra of free and bound FITC–siRNA as a function of PEG_{2000}–DMPE concentration. Fluorescence quenching of the emission peak (520–530 nm) reflects binding. (b) FITC–siRNA binding based on quenching as a function of PEG_{2000}–DMPE concentration (1 μM siRNA mM Fe^{1-} = 238 μg mg Fe^{1-}). The gray lines show the calculated PEG_{2000}–DMPE concentrations depicted in Figure 4 for the mushroom-brush transition (~10 mol % PEG–lipid) and when the brush has a similar density (~57 mol % PEG–lipid). Errors bars represent the standard deviation for n = 3.

siRNA binding. The effects of these layers were examined in HeLa human cervical carcinoma cells. Cell viability studies at 0, 15, and 50 mol % PEG–lipid demonstrated that only treatment with L-IONs with 0 mol % PEG–lipid resulted in significant loss of cell viability at L-ION concentrations greater than 5 × 10^5 L-IONs per cell (Figure 6a). Cellular toxicity was reduced with 5 mol % PEG–lipid and eliminated at 15 mol % PEG–lipid over the L-ION concentrations examined.

The colloidal stability of L-IONs in cell culture media with serum proteins (fetal bovine serum, FBS) was examined prior to in vitro studies. FBS has been shown to adsorb onto polymer-coated IONs independent of polymer charge,[35] and the presence of a protein corona can lead to aggregation, which can impact cytotoxicity and cellular uptake.[36] DLS studies were conducted in cell culture media (Opti-MEM) in the absence and presence of 10 wt % FBS (Figure 6b). L-IONs were incubated with FBS for 30 min prior to analysis. Cationic L-IONs at 0 mol % PEG–lipid exhibited aggregation in the absence of FBS, indicating charge screening in Opti-MEM resulting in aggregation. At 5, 15, and 50 mol % PEG–lipid, the L-IONs there was no significant change in size as indicated in the intensity-weighted distributions. The presence of FBS did not cause the L-IONs to aggregate, and separate peaks reflecting FBS can be seen in the DLS spectra.

Cellular uptake studies of L-IONs were performed by adding 1 mol % rhodamine lipid in the lipid coating for fluorescence imaging (Figure 6c; untreated cells are shown in Figure 6d). Overlaid bright-field and fluorescence images reflect the uptake of all three L-IONs examined. At high DOTAP concentrations, the L-IONs adsorbed onto the surface of the well plates, which

DOI: 10.1021/acs.bioconjchem.7b00483
Bioconjugate Chem. 2017, 28, 2729–2736

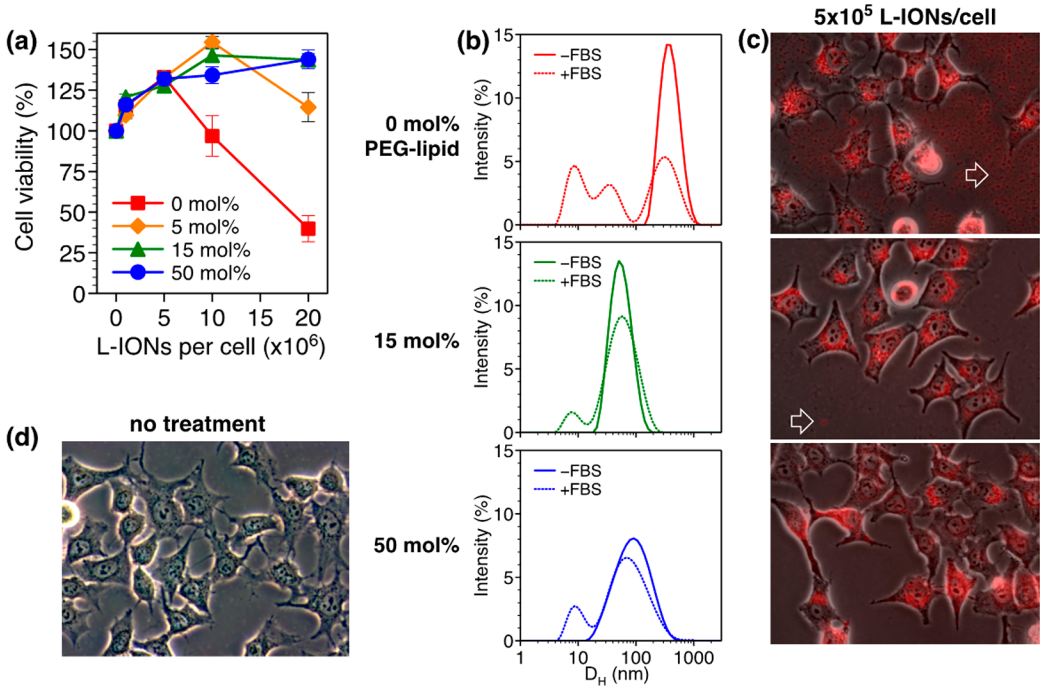

Figure 6. L-ION cytotoxicity and HeLa cell uptake. (a) Cell viability with L-IONs containing 0, 5, 15, and 50 mol % PEG–lipid. (b) Intensity-weighted size distributions of L-IONs in the absence and presence of 10 wt % FBS in Opti-MEM. (c) Inverted fluorescence and (d) phase-contrast microscopy images of L-ION-transfected HeLa cells and HeLa cells with no treatment, respectively. In panel c, L-IONs adsorbed to the well plate surface were observed at 0 and 15 mol % PEG–lipid (open white arrows) but not at 50 mol % PEG–lipid.

may have been driven by aggregation and sedimentation. Adding PEG–lipid reduced or eliminated the extent of L-ION deposition within the well plates.

HeLa cell uptake and siRNA transfection was also examined by confocal microscopy with nontargeting FITC–siRNA and by Western blot to determine protein expression with siRNA-targeting FANCD2.[23] Co-localization of L-IONs (red) and FITC–siRNA (green) was observed for each L-ION examined (Figure 7a). A direct relationship is observed between cellular uptake and siRNA binding, normalized to 0 mol % PEG–lipid, suggesting that both uptake and binding were driven by electrostatic interactions (Figure 7b); a decrease in the ratio of cationic to PEG lipids led to decreases in uptake and siRNA binding.

A reduction of ~80% was observed in FANCD2 protein expression using DOTAP L-IONs (0 mol % PEG–lipid; Figure 7c). This reduction was comparable to that for Lipofectamine 2000. L-IONs with 15 and 50 mol % exhibited similar levels protein knockdown of ~25% and 40%, respectively (a knockdown of ~25% was also observed at 5 mol % PEG–lipid). By comparing normalized protein knockdown (relative to 0 mol % PEG–lipid) to cellular uptake and siRNA binding, we observe that catanionic L-IONs with 50 mol % PEG–lipid are able to achieve appreciable protein knockdown despite exhibiting lower uptake and siRNA binding.

CONCLUSIONS

L-IONs with cationic, anionic, or catanionic lipid monolayer coatings can be formed using a dual solvent exchange technique. Because the technique yielded monodispersed L-IONs, we were able to examine the ability to tune surface charge, siRNA binding capacity, and magnetic relaxivity by varying the cationic-to-PEG–lipid ratio. Results for relaxivity and siRNA binding, where a trade-off was observed based on L-ION charge, could be tied to PEG conformation. Relaxivity (high) and siRNA binding (low) plateaued when a maximum PEG brush density was calculated near 50 mol % PEG–lipid. From these results and cell viability studies, an optimal range from 15 to 50 mol % PEG–lipid was identified, and these L-IONs were examined in vitro. At these PEG–lipid concentrations, the PEG adopted a brush conformation, and similar transfection results were observed. The approach taken in this work provides a more-complete picture of the interdependence between L-ION multifunctionalities that are affected by coating composition. Specific to this work, if the goal is to identify a coating composition in which each functionality is retained at a high level, the L-ION should be highly PEGylated with near catanionic character (equimolar mixture of cationic and anionic PEG–lipid).

EXPERIMENTAL PROCEDURES

Materials. DOTAP, PEG_{2000}–DMPE, and 1,2-dioleoyl-*sn*-glycero-3-phosphoethanolamine–*N*-(lissamine rhodamine B sulfonyl) (ammonium salt) (rhodamine–lipid) were purchased from Avanti Polar Lipids (Alabaster, AL). Oleic acid coated 30 nm IONs were purchased from Ocean NanoTech (San Diego, CA). Dimethyl sulfoxide (DMSO), agarose, 10× Tris–borate–ethylenediaminetetraacetic acid (TBE) buffer, fetal bovine serum (FBS), Opti-MEM Reduced Serum Media, Dulbecco's modified Eagle medium (DMEM), and Vivaspin 2 100 kDa molecular weight cutoff centrifuge tubes (GE Health) were purchased from Fisher Scientific (Suwanee, GA). Fluorescein (FAM)-labeled negative control siRNA (21 base pairs) was purchased from Shanghai GenePharma Co., Ltd. (Shanghai, China). Sterile deionized ultrafiltered (DI) water at 18.2 mΩ was used from a Millipore Direct-Q3 UV purification system (Billerica, MA).

DOI: 10.1021/acs.bioconjchem.7b00483
Bioconjugate Chem. 2017, 28, 2729–2736

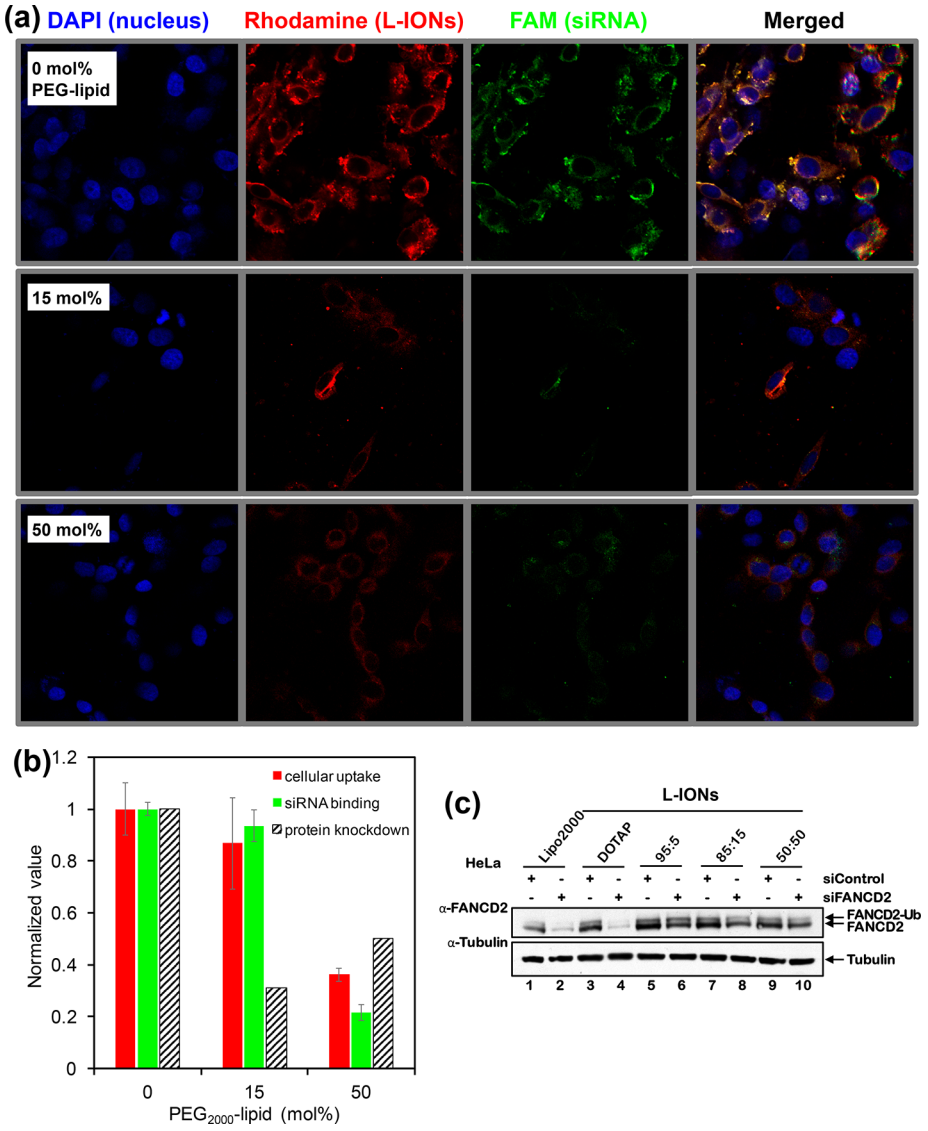

Figure 7. L-ION HeLa cell uptake, siRNA transfection, and protein expression. (a) Confocal microscopy images are shown for HeLa cells (stained with DAPI, blue), L-IONs (stained with Rhodamine lipid, red), and siRNA (nontargeting FAM-labeled, green). The L-ION concentration was 5×10^5 L-IONs per cell. Merged images show L-ION internalization and co-localization. (b) Comparison of cellular uptake, determined by fluorescence intensity per HeLa cell, siRNA binding, and FANCD2 protein knockdown. (d) Western blot for FANCD2 protein expression in HeLa cells transfected with control nontargeting siRNA or FANCD2-targeting siRNA using Lipofectamine 2000 or L-IONs with the indicated DOTAP-to-PEG−lipid ratios. A total of 72 h following transfection, cells were harvested and proteins analyzed by immunoblotting with anti-FANCD2 and anti-Tubulin antibodies.

L-ION Formation. L-IONs were formed with DOTAP-to-PEG−lipid ratios from 100:0 to 0:100 using a dual solvent exchange method.[24] Lipids and IONs were mixed in chloroform at a lipid-to-Fe weight ratio of 32:1 in a round-bottom flask. For rhodamine-labeled L-IONs, rhodamine−lipid was also added at 0.6 mol % of total lipids. DMSO, equal to four times the volume of chloroform, was then added to the flask in 50 μL aliquots under bath sonication. The flask was gently shaken for 30 min. Chloroform was removed by rotary evaporation at room temperature (RT) at 200 mbar for 35 min and then 50 mbar for 30 min. DI water (2−3 mL) was added at 0.2 mL min^{-1}, and the samples were placed in membrane centrifuge tubes and centrifuged at 20 °C and 7000g for 30 min. DI water (1 mL) was then added to each tube using pipet mixing to remove L-IONs from the membrane, and the sample was centrifuged again. This was repeated twice before the final L-IONs suspension was obtained. Excess lipids were removed by centrifugation at 18516g for 15 min at RT. The supernatant was removed and discarded, and the precipitate was resuspended in the desired volume of DI water by vortex mixing.

Cryogenic Transmission Electron Microscopy. L-IONs were examined by cryo-TEM imaging. Specimens were prepared by depositing a 5 μL sample onto a Quantifoil grid composed of 200 square mesh copper grids suspended with 2 μm holey carbon (Electron Microscopy Sciences, Hatfield, PA). The sample grids were robotically vitrified in liquid ethane using a Vitrobot (FEI Company, Hillsboro, OR). Prior to imaging, the vitrified grid was transferred to and stored in liquid nitrogen. Imaging was performed in a liquid nitrogen cooled stage (Model 915, Gatan Inc., Pleasonton, CA) at 200 kV using a JEOL JEM-2100F TEM (Peabody, MA).

DOI: 10.1021/acs.bioconjchem.7b00483
Bioconjugate Chem. 2017, 28, 2729−2736

Dynamic Light Scattering. Number-averaged hydrodynamic diameter, D_H, and ζ potential, e, was determined using a Malvern Zetasizer Nano ZS (Worcestershire, United Kingdom) equipped with a backscattering detector angle of 173° and a 4 mW, 633 nm He−Ne laser. ζ potential was determined by combined Doppler electrophoretic velocimetry and phase-analysis light scattering using folded capillary cells.

siRNA Binding. FAM-siRNA binding to L-IONs was determined by fluorescence spectroscopy based on previous studies that have shown that cationic lipids quench the fluorescence of fluorophore-labeled siRNAs.[33,34] Fluorescence intensity was measured with a PerkinElmer Model LS 55 fluorescence spectrometer (Waltham, MA) with excitation and emissions slit widths of 10 nm, a 1% attenuation filter, and excitation and emission wavelengths of 494 and 516 nm, respectively. For in situ measurements, Opti-MEM buffer was first added to a quartz cuvette and the intensity, I_{buffer}, was recorded. FAM−siRNA was then added yielding I_{siRNA}. Finally, L-IONs were added and the intensity, $I(t)$, was integrated over 10 s intervals and recorded over 15 min. The percent of bound siRNA was calculated as $[I_{siRNA} - I(t)]/[I_{siRNA} - I_{buffer}]$. To ensure that quenching was due to L-IONs, samples were then transferred to centrifuge tubes and centrifuged at 6000*g* for 15 min to isolate bound (sediment) and unbound siRNA (supernatant). The supernatant was analyzed ex situ and compared to the in situ measurements.

MRI Relaxivity. L-IONs were suspended in 1% agarose at concentrations of 1, 10, and 20 μg Fe_3O_4 mL^{-1} in 4 mL plastic sample tubes. Agarose gels were prepared by mixing agarose with 10× TBE buffer (diluted to 1X) in a flask on a hot plate set to keep the gel at 80 °C until the agarose is completely dissolved. The L-ION/gel sample was then vortexed and stored at 4 °C until analysis.

The magnetic relaxivity of L-IONs was measured using a Siemens Prisma 3T scanner. Samples were placed in a 64 channel head receive array and scanned using spin echo (for assessment of r_2). Cross-section images of the vials were obtained with voxel size of 0.78 mm and slice thickness of 4 mm. Repetition time was 2400 ms for all sequences. For the spin echo acquisition, 24 echoes were collected over the range of 9−216 ms (9 ms steps). The inversion recovery data were taken with inversion times of 100, 200, 300, 400, 600, 1000, and 1500 ms. Relaxation time constants were determined using a nonlinear least-squares fit for pixel intensity as a function of echo time for r_2 and as a function of inversion time for r_1. Nonlinear least-squares fitting routines with three parameters (M_0, $T_{1,2}$, and DC offset) were used to take into account offset effects from noise and detector calibration. Relaxivity was calculated as a linear fit of relaxation rates to Fe concentration.

Cytotoxicity Assay. HeLa cells were plated at a density of 10 000 cells in a 96-well dish. A total of 24 h later, cells were treated with varying concentrations of L-IONs. After 48 h, CellTiter 96 AQ_{aeous} One Solution Reagent (MTS) (Promega) was added directly to the wells, cells were incubated with shaking for a further 2 h, and the absorbance at 490 nm was measured using a 96-well Bio-Rad 680 microplate reader. Percentage survival was calculated in relation to untreated cells.

siRNA Delivery. A single day prior to transfection, HeLa cells were plated at a density of 150 K per well in 6-well dishes or 20 000 per chamber slide for confocal microscopy. The following day, 5×10^5 L-IONs per cell were incubated with Opti-MEM for 15 min at RT. siRNA with the following sense and antisense sequences were incubated with Opti-MEM to a final concentration of 200 nM for 15 min, FAM−siRNA (GenePharma) 5′-UUCUCCGAACGUGUCACGUTT-3′, and 5′-UUACGUGACACGUUCGGAGAA-3′, siFANCD2 (Dharmacon) 5′-CAGCCUACCUGAGAUCCUA-3′ and 5′- UAGGAUCUCAGGUAGGCUG-3′ or nontargeting siCtrl (Dharmacon) 5′- UAACGACGCGACGACGUAA-3′ and 5′-UUACGUCGUCGCGUCGUUA-3′. L-ION/OptiMEM and siRNA/Opti-MEM mixtures were added together and incubated for 15 min at RT and added to cells. Cells were returned to 37 °C for 8 h. DMEM complete was added to cells and they were returned to the incubator. Fluorescent imaging of live cells was taken 24 h after transfection with a Zeiss Axio Imager A1 and Vision Rel. 4.6, Dell Optiplex 735. For confocal microscopy, cells were fixed with 4% paraformaldehyde and 2% sucrose for 15 min, permeabilized with 0.3% v/v Triton-X-100 in PBS, counterstained with DAPI (406-diamidine-2-phenylindole dihydrochloride), and imaged with a Zeiss Axio Imager M2 with Zeiss ZEN 2011 software. For siRNA knockdown, media was replaced after 24 h, and cells were allowed to grow for 72 h post-transfection. Cells were harvested and lysed in 2% sodium dodecyl sulfate (SDS) lysis buffer (50 mM Tris·Cl, pH 7.5, 10 mM EDTA, 2% v/v SDS). Proteins were resolved on NuPage 3−8% w/v Tris−acetate or 4−12% w/v Bis−Tris gels (Invitrogen) and transferred to polyvinylidene difluoride membranes, followed by immunoblotting with anti-FANCD2 (NB100−182, Novus Biologicals) and anti-Tubulin (MS-581-PO, Lab Vision) antibodies.

AUTHOR INFORMATION

Corresponding Author

*E-mail: gbothun@uri.edu. Phone: +1-401-874-9518.

ORCID

Geoffrey D. Bothun: 0000-0002-7513-2417

Notes

The authors declare no competing financial interest.

ACKNOWLEDGMENTS

We gratefully acknowledge Yanjing Chen, Yaser Kashcooli, Timothy Ryan Lynn, Andrea Villarroel, and Kyle Mummau for their contributions to this work. This material is based on work supported by the National Science Foundation (NSF) under grant nos. CBET-0931875 and CBET-1337061. Additional resources were provided by the URI Genomics Sequencing Center (RI NSF EPSCoR grant no. OIA-1004057), the MRI Facility in the Brain Institute at Brown University, the Electron Microscopy Facilities in the RI Consortium for Nanoscience and Nanotechnology, the National Institutes of Health and the National Heart, Lung and Blood Institute (grant no. R01HL101977), and the Rhode Island IDeA Network of Biomedical Research Excellence (RI-INBRE; grant no. P20GM103430 from the National Institute of General Medical Sciences).

REFERENCES

(1) Laurent, S., Forge, D., Port, M., Roch, A., Robic, C., Elst, L. V., and Muller, R. N. (2008) Magnetic iron oxide nanoparticles: Synthesis, stabilization, vectorization, physicochemical characterizations, and biological applications. *Chem. Rev. 108*, 2064−2110.

(2) Mornet, S., Vasseur, S., Grasset, F., and Duguet, E. (2004) Magnetic nanoparticle design for medical diagnosis and therapy. *J. Mater. Chem. 14*, 2161−2175.

(3) Zhu, L., Zhou, Z., Mao, H., and Yang, L. (2017) Magnetic nanoparticles for precision oncology: theranostic magnetic iron oxide

DOI: 10.1021/acs.bioconjchem.7b00483
Bioconjugate Chem. 2017, 28, 2729−2736

nanoparticles for image-guided and targeted cancer therapy. *Nanomedicine 12*, 73−87.
(4) Revia, R. A., and Zhang, M. Q. (2016) Magnetite nanoparticles for cancer diagnosis, treatment, and treatment monitoring: recent advances. *Mater. Today 19*, 157−168.
(5) Hergt, R., Dutz, S., Muller, R., and Zeisberger, M. (2006) Magnetic particle hyperthermia: nanoparticle magnetism and materials development for cancer therapy. *J. Phys.: Condens. Matter 18*, S2919.
(6) Kang, T., Li, F., Baik, S., Shao, W., Ling, D., and Hyeon, T. (2017) Surface design of magnetic nanoparticles for stimuli-responsive cancer imaging and therapy. *Biomaterials 136*, 98−114.
(7) Tromsdorf, U. I., Bigall, N. C., Kaul, M. G., Bruns, O. T., Nikolic, M. S., Mollwitz, B., Sperling, R. A., Reimer, R., Hohenberg, H., Parak, W. J., Forster, S., Beisiegel, U., Adam, G., and Weller, H. (2007) Size and surface effects on the MRI relaxivity of manganese ferrite nanoparticle contrast agents. *Nano Lett. 7*, 2422−7.
(8) Duan, H. W., Kuang, M., Wang, X. X., Wang, Y. A., Mao, H., and Nie, S. M. (2008) Reexamining the effects of particle size and surface chemistry on the magnetic properties of iron oxide nanocrystals: New insights into spin disorder and proton relaxivity. *J. Phys. Chem. C 112*, 8127−8131.
(9) Hajesmaeelzadeh, F., Shanehsazzadeh, S., Gruttner, C., Daha, F. J., and Oghabian, M. A. (2016) Effect of coating thickness of iron oxide nanoparticles on their relaxivity in the MRI. *Iran J. Basic Med. Sci. 19*, 166−171.
(10) LaConte, L. E. W., Nitin, N., Zurkiya, O., Caruntu, D., O'Connor, C. J., Hu, X. P., and Bao, G. (2007) Coating thickness of magnetic iron oxide nanoparticles affects R2 relaxivity. *J. Magn Reson Imaging 26*, 1634−1641.
(11) Tong, S., Hou, S., Zheng, Z., Zhou, J., and Bao, G. (2010) Coating Optimization of Superparamagnetic Iron Oxide Nanoparticles for High T2 Relaxivity. *Nano Lett. 10*, 4607−4613.
(12) Chen, Y. J., Tao, J. A., Xiong, F., Zhu, J. B., Gu, N., Zhang, Y. H., Ding, Y., and Ge, L. A. (2010) Synthesis, self-assembly, and characterization of PEG-coated iron oxide nanoparticles as potential MRI contrast agent. *Drug Dev. Ind. Pharm. 36*, 1235−1244.
(13) Huang, H. C., Chang, P. Y., Chang, K., Chen, C. Y., Lin, C. W., Chen, J. H., Mou, C. Y., Chang, Z. F., and Chang, F. H. (2009) Formulation of novel lipid-coated magnetic nanoparticles as the probe for in vivo imaging. *J. Biomed. Sci. 16*, 86.
(14) Namiki, Y., Namiki, T., Yoshida, H., Ishii, Y., Tsubota, A., Koido, S., Nariai, K., Mitsunaga, M., Yanagisawa, S., Kashiwagi, H., Mabashi, Y., Yumoto, Y., Hoshina, S., Fujise, K., and Tada, N. (2009) A novel magnetic crystal−lipid nanostructure for magnetically guided in vivo gene delivery. *Nat. Nanotechnol. 4*, 598.
(15) Jiang, S., Eltoukhy, A. A., Love, K. T., Langer, R., and Anderson, D. G. (2013) Lipidoid-coated iron oxide nanoparticles for efficient DNA and siRNA delivery. *Nano Lett. 13*, 1059−64.
(16) Perry, J. L., Reuter, K. G., Kai, M. P., Herlihy, K. P., Jones, S. W., Luft, J. C., Napier, M., Bear, J. E., and DeSimone, J. M. (2012) PEGylated PRINT nanoparticles: the impact of PEG density on protein binding, macrophage association, biodistribution, and pharmacokinetics. *Nano Lett. 12*, 5304−10.
(17) Rabanel, J. M., Hildgen, P., and Banquy, X. (2014) Assessment of PEG on polymeric particles surface, a key step in drug carrier translation. *J. Controlled Release 185*, 71−87.
(18) Moghimi, S. M., and Szebeni, J. (2003) Stealth liposomes and long circulating nanoparticles: critical issues in pharmacokinetics, opsonization and protein-binding properties. *Prog. Lipid Res. 42*, 463−78.
(19) Kanasty, R., Dorkin, J. R., Vegas, A., and Anderson, D. (2013) Delivery materials for siRNA therapeutics. *Nat. Mater. 12*, 967−77.
(20) Verma, A., and Stellacci, F. (2010) Effect of Surface Properties on Nanoparticle-Cell Interactions. *Small 6*, 12−21.
(21) Pillai, P. P., Huda, S., Kowalczyk, B., and Grzybowski, B. A. (2013) Controlled pH Stability and Adjustable Cellular Uptake of Mixed-Charge Nanoparticles. *J. Am. Chem. Soc. 135*, 6392−6395.
(22) Wang, T., Upponi, J. R., and Torchilin, V. P. (2012) Design of multifunctional non-viral gene vectors to overcome physiological barriers: Dilemmas and strategies. *Int. J. Pharm. 427*, 3−20.
(23) Howlett, N. G., Taniguchi, T., Durkin, S. G., D'Andrea, A. D., and Glover, T. W. (2005) The Fanconi anemia pathway is required for the DNA replication stress response and for the regulation of common fragile site stability. *Hum. Mol. Genet. 14*, 693−701.
(24) Tong, S., Hou, S., Ren, B., Zheng, Z., and Bao, G. (2011) Self-assembly of phospholipid-PEG coating on nanoparticles through dual solvent exchange. *Nano Lett. 11*, 3720−6.
(25) Fenyves, R., Schmutz, M., Horner, I. J., Bright, F. V., and Rzayev, J. (2014) Aqueous self-assembly of giant bottlebrush block copolymer surfactants as shape-tunable building blocks. *J. Am. Chem. Soc. 136*, 7762−70.
(26) Wang, Y. X. (2011) Superparamagnetic iron oxide based MRI contrast agents: Current status of clinical application. *Quant Imaging Med. Surg 1*, 35−40.
(27) Estelrich, J., Sanchez-Martin, M. J., and Busquets, M. A. (2015) Nanoparticles in magnetic resonance imaging: from simple to dual contrast agents. *Int. J. Nanomed. 10*, 1727−41.
(28) de Haan, H. W., and Paquet, C. (2011) Enhancement and degradation of the R2* relaxation rate resulting from the encapsulation of magnetic particles with hydrophilic coatings. *Magn. Reson. Med. 66*, 1759−66.
(29) Vuong, Q. L., Berret, J. F., Fresnais, J., Gossuin, Y., and Sandre, O. (2012) A Universal Scaling Law to Predict the Efficiency of Magnetic Nanoparticles as MRI T2-Contrast Agents. *Adv. Healthcare Mater. 1*, 502−512.
(30) Gillis, P., Roch, A., and Brooks, R. A. (1999) Corrected equations for susceptibility-induced T2-shortening. *J. Magn. Reson. 137*, 402−7.
(31) Issa, B., Qadri, S., Obaidat, I. M., Bowtell, R. W., and Haik, Y. (2011) PEG coating reduces NMR relaxivity of Mn(0.5)Zn(0.5)-Gd(0.02)Fe(1.98)O4 hyperthermia nanoparticles. *J. Magn Reson Imaging 34*, 1192−8.
(32) Aguilar-Castillo, B. A., Santos, J. L., Luo, H., Aguirre-Chagala, Y. E., Palacios-Hernandez, T., and Herrera-Alonso, M. (2015) Nanoparticle stability in biologically relevant media: influence of polymer architecture. *Soft Matter 11*, 7296−307.
(33) Kheirolomoom, A., Kim, C. W., Seo, J. W., Kumar, S., Son, D. J., Gagnon, M. K. J., Ingham, E. S., Ferrara, K. W., and Jo, H. (2015) Multifunctional Nanoparticles Facilitate Molecular Targeting and miRNA Delivery to Inhibit Atherosclerosis in ApoE(−/−) Mice. *ACS Nano 9*, 8885−8897.
(34) Vader, P., van der Aa, L. J., Engbersen, J. F. J., Storm, G., and Schiffelers, R. M. (2010) A method for quantifying cellular uptake of fluorescently labeled siRNA. *J. Controlled Release 148*, 106−109.
(35) Sakulkhu, U., Mahmoudi, M., Maurizi, L., Salaklang, J., and Hofmann, H. (2015) Protein Corona Composition of Superparamagnetic Iron Oxide Nanoparticles with Various Physico-Chemical Properties and Coatings. *Sci. Rep. 4*, 1 DOI: 10.1038/srep05020.
(36) Lee, Y. K., Choi, E. J., Webster, T. J., Kim, S. H., and Khang, D. (2015) Effect of the protein corona on nanoparticles for modulating cytotoxicity and immunotoxicity. *Int. J. Nanomed. 10*, 97−113.

DOI: 10.1021/acs.bioconjchem.7b00483
Bioconjugate Chem. 2017, 28, 2729−2736